JOURNAL OF Applied Polymer SCIENCE

Transport Properties of Sulfonated Poly (styrene-isobutylene-styrene) Membranes with Counter-Ion Substitution

Sonia L. Avilés-Barreto, David Suleiman
Chemical Engineering Department, University of Puerto Rico, Mayagüez, Puerto Rico, 00681-9000
Correspondence to: D. Suleiman (E-mail: david.suleiman@upr.edu)

ABSTRACT: In this study, the transport properties of poly(styrene-isobutylene-styrene) (SIBS) were determined as a function of sulfonation level (0–94.9%) and counter-ion substitution (Ba^{+2}, Ca^{+2}, Mg^{+2}, Mn^{+2}, Cu^{+2}, K^{+1}) for fuel cell applications. Increasing the sulfonation level improved the ion exchange capacity (IEC) of the membranes up a maximum (1.71 mequiv/g), suggesting a complex three-dimensional network at high sulfonation levels. Results show that proton conductivity increases with IEC and is very sensitive to hydration levels. Methanol permeability, although also sensitive to IEC, shows a different behavior than proton conductivity, suggesting fundamental differences in their transport mechanism. The incorporation of counter-ion substitution decreases both methanol and proton transport. Methanol permeability seems to be related to the size of the counter-ion studied, while proton conductivity is more sensitive to water content, which is also reduced upon the incorporation of counter-ions. To complement the studies, selectivity (i.e., proton conductivity/methanol permeability) of the studied membranes was determined and compared to Nafion® 117. © 2013 Wiley Periodicals, Inc. J. Appl. Polym. Sci. 000: 000–000, 2013

KEYWORDS: cross-linking; nanostructured polymers; structure–property relations; batteries and fuel cells; functionalization of polymer

Received 12 June 2012; accepted 13 December 2012; published online
DOI: 10.1002/app.38952

INTRODUCTION

Many applications are known for proton exchange membranes (PEM's), especially in the area of energy efficient and electrochemical devices such as fuel cells.[1–6] The most commonly used PEM is Nafion®.[1–3,7–9] This perfluorosulfonic PEM gives high proton conductivity and good mechanical and thermal stability,[8–11] but it has several disadvantages, such as poor selectivity, high methanol permeation rates, limited processability due to the perfluorinated segments and high cost, limiting existing devices.

To meet the requirements of high ionic conductivity with proper chemical, thermal, and mechanical strength and to overcome the transport issues, a variety of block copolymers have been studied and characterized to explore their properties.[6,12,13] They can be grouped into: perfluorinated ionomeric membranes (e.g., Nafion®, Flemion®, polyvinylidene fluoride-hexafluoropropylene), non-fluorinated hydrocarbons (aliphatic and aromatic) ionomeric membranes (e.g., polystyrenesulfonic acid, sulfonated polystyrene-ethylene-butylene-polystyrene, sulfonated polyphenylene oxide, sulfonated polyether ketone ketone), and acid–base complexes (e.g., phosphoric acid-doped polybenzimidazole).[1,6,7,12,14–18]

Hydrocarbon polymers containing polar groups, as sulfonic groups ($-SO_3^-$), which retain high amounts of water over a wide temperature range are particularly attractive and relatively cheaper to synthesize than perfluorinated polymers.[18,19] Sulfonic groups can be added to hydrocarbon polymers that have an aromatic ring on their backbone by post-sulfonation using aromatic electrophilic substitution. Incorporation of this sulfonic groups increase properties like strength, hydrophilicity, and proton conductivity.[20,21] Sulfonated copolymers, with an elastomeric block, have gained interest because they combine properties of two materials and have a highly ordered sequence of both ionic and non-ionic blocks, since only one of the blocks is sulfonated.[22] On the ionic blocks phase segregation can occur due to the electrostatic interaction among ion pairs forming ion clusters. As the ionic domains increase, due to the increment of sulfonic groups, these clusters connect forming ionic channels that facilitate the transport of protons.[1,20] On the other hand, the non-ionic domains could be designed to be effective barriers for methanol (MeOH).[1]

Previous studies have characterized sulfonated poly(styrene-isobutylene-styrene) (SIBS) and evaluated their potential as a viable PEM for fuel cells and protective clothing applications.[2,20,23] SIBS is a tri-block thermoplastic elastomer which is composed of glassy outer blocks (polystyrene) and rubbery inner blocks [poly(isobutylene)].[24,25] By sulfonating the polystyrene blocks, an ionomer that self assembles into a three-phase

© 2013 Wiley Periodicals, Inc.

nanostructured morphology in the solid state and a polymer that combines ionic and non-ionic properties can be produced.[26] To increase its selectivity ionic cross-linking is suggested. One approach is to exchange with cations some of the protons in the acidic membranes. The cation-substituted membrane produced by the exchange reaction should have very low water solubility and form a stable cross-link that can enhance properties as transition temperatures, plateau modulus and tensile strength. Also, it can reduce the solvent swelling and methanol permeability.[16] This study presents the synthesis and characterization of SIBS with respect to two major variables: sulfonation level and counter-ion substitution. The transport properties of the resulting PEM's have been evaluated and the results have been explained using an in-depth materials characterization approach.

EXPERIMENTAL

Materials

SIBS was purchased from Kaneka® with properties of 30 wt % polystyrene and a molecular weight of 65,000 g/mol. Other chemicals used include: methylene chloride (Fisher Scientific, 99.8%), sulfuric acid (Sigma Aldrich, 95–98%), acetic anhydride (Aldrich Chemical, 99+%), toluene (Fisher Scientific, 99.8%), hexyl alcohol (Aldrich Chemical, 98%), methanol (Fisher Scientific, 99.9%), barium chloride (Sigma–Aldrich, anhydrous, powder, 99.99%), calcium chloride (Sigma–Aldrich, anhydrous, powder, 99.99%), magnesium chloride (Sigma–Aldrich, anhydrous, powder, 99.99%), manganese chloride ($MnCl_2$) (Acros Organics, 99+%), copper (II) chloride ($CuCl_2$) (Across Organics, anhydrous, 99%), potassium chloride (KCl) (Fisher Scientific), and deionized (DI) water. All chemicals were used without further purification.

Polymer Sulfonation

The sulfonation of SIBS was performed using the suggested procedure of Elabd and Napadensky.[1,20] Some modifications were considered, an example of the sulfonation procedure is as follows: a 10% (wt/v) solution of SIBS (30 g dried for 24 h at 60°C) in methylene chloride was prepared. The sulfonating agent, acetyl sulfate, in methylene chloride is prepared by cooling 200 mL of methylene chloride in an ice bath for 10 min, and then acetic anhydride is added to the methylene chloride under stirring conditions. The cooling is to account for the exothermic heat of reaction, while avoiding solvent evaporation. Sulfuric acid is added 10 min after the acetic anhydride with an acetic anhydride mole ratio of 1 : 1. The sulfonating agent was slowly added to the polymer solution to begin the sulfonation reaction. The reaction was terminated after 24 h by adding 200 mL of methanol and the solvents were allowed to evaporate at room temperature for 5 days. The reacted polymer was washed several times with DI water until the pH of the water was neutral. The used water with residual acetyl sulfate was neutralized with sodium hydroxide minimizing the waste produced in this process. Since the concentration of acetic acid produced after neutralization is lower than the allowed disposable limit, the neutralized water was safe to discard. The polymer was then dried at 60°C for 48 h. The sulfonation procedure was repeated several times with different amounts of acetyl sulfate to obtain various sulfonating levels. Higher sulfonation levels require a larger excess of the sulfonation agent, since upon sulfonation ionic nanochannels are formed and it is difficult to overcome the mass-transport limitations to reach the last unoccupied sites available for sulfonation.

Membrane Casting

Once sulfonated SIBS was pH balanced and dried it was dissolved in a solution (85/15) (v/v) of toluene and hexyl alcohol with a polymer concentration of 5 wt %. SIBS membranes were solvent casted in Teflon® Petri dishes for 1 week at room temperature allowing for the membranes to thermodynamically self-assemble as the solvent evaporated. They were then dried at 60°C for 24 h to remove the final residual solvent. The unsulfonated polymer was casted similarly, but with pure toluene instead.

Counter-Ion Substitution

The membranes were neutralized by immersing the sulfonated membranes in acid form in 1.0*M* solution of the salts containing the desired cation ($BaCl_2$, $CaCl_2$, $MgCl_2$, $MnCl_2$, $CuCl_2$, and KCl) for 24 h. The cation substitution takes place in a few minutes for thin membranes (e.g., 0.1 cm), but they were immersed for 24 h to allow for proper cation substitution. The cross-linked membranes were then washed using DI water and dried in an oven at 60°C for 24 h.

Nomenclature

The membranes were labeled SIBS–XX–Y^Z, indicating SIBS polymer followed by XX, which is the sulfonation mole percent obtained after elemental analysis (EA), Y, which is the cation substituted, and Z, which is the cation electrical charge before the substitution.

Materials Characterization

EA was performed by Atlantic Microlab (Norcross, GA) to determine accurate sulfonation levels. Sulfonated membrane samples (1–3 mg) were analyzed for carbon, hydrogen, and sulfur weight percent. Additional stoichiometric calculations were required to obtain the final mole percent of sulfonation for all the membranes studied.

Instrumental neutron activation analysis (INAA) was performed by Elemental Analysis (Lexington, KY) to determine the amount of cations substituted. Cross-linked membrane samples of approximately 0.1 g were analyzed for sulfur and cation composition. Results are presented as the mole ratio between cation and sulfonic groups.

Ion exchange capacity (IEC) was measured immersing 50 mg of the sulfonated membrane in a 1.0*M* solution of NaCl for 24 h. After removing the membrane, the solution was titrated using a 0.1*M* solution of NaOH until the pH was neutral. The IEC was calculated from the moles of ion substituted divided by the initial dry mass of the membrane.

Fourier transform infrared spectroscopy (FT-IR) was used to confirm the presence of sulfonic groups and determine their aromatic substitution configuration. Infrared spectrums of the samples were collected using a Varian (Palo Alto, CA) 800 FTIR Scimitar Series Spectrometer and a ZnSe ATR holder with a wavenumber range of 600–4000 cm^{-1} using 100 scans at 8 cm^{-1} resolution.

Table I. Counter-Ion Concentration in the Cross-linked Membranes by INNA

	Cation mass fraction per sulfonic group					
Sample	Ba^{+2}	Ca^{+2}	Mg^{+2}	Mn^{+2}	$Cu+^{2}$	K^{+1}
SIBS 39.8	0.4235	0.4801	0.4900	0.4540	0.4100	0.8423
SIBS 63.1	0.3759	0.5667	0.4915	0.4525	0.4428	0.7245
SIBS 84.1	0.3595	0.5015	0.4947	0.4548	0.3657	0.9439

The thermal stability and degradation temperatures of the samples were determined using a TGA/SDTA 851 from Mettler Toledo (Columbus, OH) by heating the samples to 800°C at a constant heating rate of 10°C/min under a nitrogen atmosphere.

To confirm the assignments of the degradation temperatures and determine the composition of the remaining mass, a TGA 2950 Thermogravimetrical Analyzer (TA Instruments, New Castle, DE) coupled to a Thermo Scientific TGA-FTIR interface was used under a helium atmosphere in a temperature range of 25–850°C at a heating rate of 15°C/min. The gas cell temperature was set to 220°C and the transfer line to 210°C.

Structure–property relations for dry sulfonated and counter-ion substituted membranes were determined using small-angle X-ray scattering (SAXS). The experiments were performed in the Chemical Engineering Department of the University of Washington, Seattle using a one dimension SAXSess mc^2 and SAXSquanTM-Software for the data analysis.

Transmission electron microscopy (TEM) was used to obtain an image of the polymer membrane upon sulfonation. The experiments were performed in the Nanotechnology User Facility of the University of Washington, Seattle using a FEI Tecnai G2 F20 TEM. The samples were spin-coated at 4000 rpm for one minute onto Carbon B copper grits (Ted Pella).

Solvent swelling experiments were performed to determine absorption limitations and their effect on the membrane transport. For swelling measurements, square samples of the membranes were dried at 60°C for 24 h, weighted and then immersed into vials containing DI water. The weight of wet membranes was determined, after removing the surface solvent by blotting it with a tissue paper, at different times until equilibrium was reached.

Transport Properties

In-plane ion conductivity for each membrane was measured using electrochemical impedance spectroscopy (EIS) over a frequency range of 0.1 Hz and 1 MHz with an applied voltage of 10 mV (AC Solartron impedance system: 1260 impedance analyzer, 1287 electrochemical interface, Zplot software). Membranes were cut into 3 × 0.5 cm strips and submerged in DI water for at least 24 h before the conductivity measurements were performed. The membrane strips were then loaded in hydrated form into an open cell consisting of four Pt parallel electrodes. Conductivities of the membranes were measured at room temperature (~ 25°C), where the cell was filled with DI water to maintain full hydration of the membranes during the measurements. The real impedance was calculated from the x-intercept of the regression of Nyquist plot. In-plane conductivity, σ (S/cm), was calculated with eq. (1), where L_e is the distance between electrodes, R is the real impedance or resistance (Ω), and A is the cross sectional area. Wet membrane thickness and width were measured directly after the membrane was removed from the conductivity cell. The membrane thickness and width changed upon hydration and the changes varied with sulfonation level and counter-ion substitution; however, changes in width were more significant than changes in thickness. Additional details concerning the apparatus and procedures can be found elsewhere.[27,28]

$$\sigma = \frac{L_e}{(AR)} \tag{1}$$

Methanol permeability was measured at room temperature using a side-by-side diffusion cell. Membranes were prior hydrated with DI water for 24 h and then put between both sides of the cell, each one with a compartment of 0.3215 cm^2 of cross-sectional area. The donor compartment was filled with a 2.0*M* MeOH solution and the receptor with DI water. Infrared spectra from the receptor compartment was recorded every 10 min using 100 scans and 8 cm^{-1} resolution. The concentration of methanol was obtained by monitoring the C—O stretching of 1014 cm^{-1}. In addition, a GC-TCD (Shimadzu, GC-8) was used to corroborate the accuracy of the FT-IR technique. Methanol permeability was determined using the rearranged approximate solution of the continuity equation [eq. (2)] for diffusion in plane sheet geometry (constant concentration in one side).[1,29] Where C_A and C_B are the concentration of methanol in the donor and receptor compartments, respectively, L is the membrane thickness (0.03–0.08 cm), V_B the volume of the receptor compartment (0.37 cm^3), A the cross-sectional area of the membrane

Table II. Sulfonation Percentage and Ion Exchange Capacity for Sulfonated SIBS Membranes

Sample	Sulfonation level (mol %)	IEC (mequiv./g)
SIBS 29.7	29.7	0.77
SIBS 39.8	39.8	1.06
SIBS 63.1	63.1	1.69
SIBS 84.1	84.1	1.71
SIBS 92.0	92.0	1.57

Applied Polymer SCIENCE

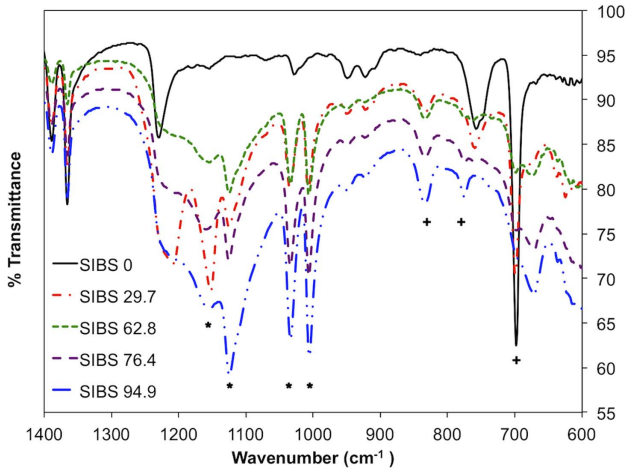

Figure 1. Infrared spectra of SIBS at various sulfonation levels (0, 29.7, 62.8, 76.4, and 94.9 mol %). The mark peaks represent stretching vibrations associated to sulfonated group (*) and the aromatic substitution (+). [Color figure can be viewed in the online issue, which is available at wileyonlinelibrary.com.]

(0.322 cm^2), D is the methanol diffusion coefficient (cm^2/s), and P the permeability (cm^2/s). The permeability represents the product of the diffusion coefficient times the solubility.[29]

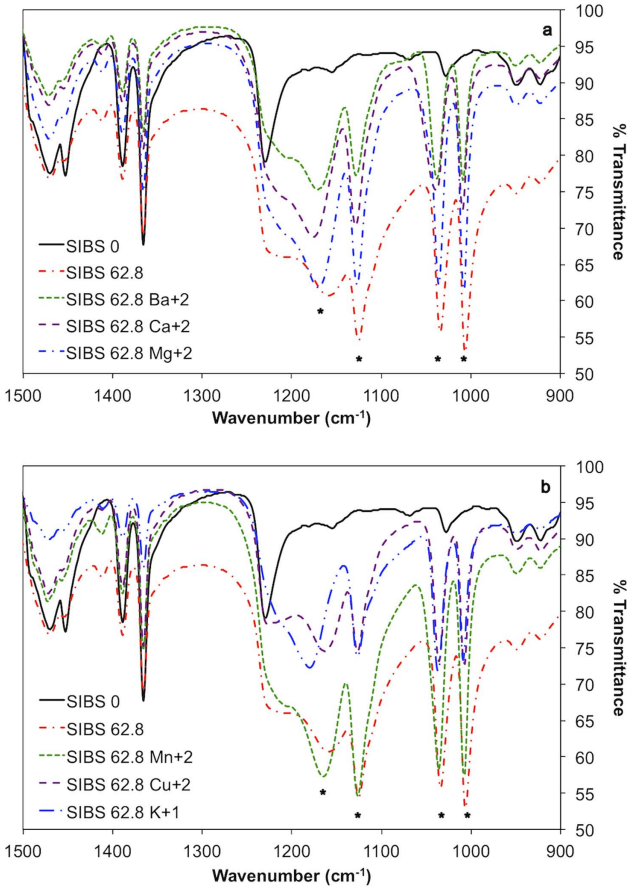

Figure 2. Infrared spectra of SIBS 62.8 cross-linked with various counter ions: (a) Ba^{+2}, Ca^{+2}, Mg^{+2}, and (b) Mn^{+2}, Cu^{+2}, K^{+1}. [Color figure can be viewed in the online issue, which is available at wileyonlinelibrary.com.]

Table III. FTIR Stretching Vibration Bands for Sulfonated and Cross-linked SIBS Membranes

Sample	FTIR stretching bands (cm^{-1})			
SIBS 0	–	–	–	–
SIBS 29.7	1007	1034	1124	1151
SIBS 62.8	1007	1034	1124	1153
SIBS 76.4	1007	1034	1124	1159
SIBS 94.9	1007	1034	1124	1153
SIBS 29.7 Ba^{+2}	1009	1038	1126	1169
SIBS 62.8 Ba^{+2}	1009	1038	1128	1171
SIBS 94.9 Ba^{+2}	1009	1038	1128	1169
SIBS 29.7 Ca^{+2}	1009	1038	1128	1177
SIBS 62.8 Ca^{+2}	1009	1038	1128	1177
SIBS 94.9 Ca^{+2}	1009	1038	1128	1175
SIBS 29.7 Mg^{+2}	1009	1036	1126	1165
SIBS 62.8 Mg^{+2}	1009	1036	1126	1171
SIBS 94.9 Mg^{+2}	1009	1036	1126	1171
SIBS 29.7 Mn^{+2}	1009	1036	1126	1155
SIBS 62.8 Mn^{+2}	1009	1036	1126	1165
SIBS 94.9 Mn^{+2}	1007	1036	1126	1165
SIBS 29.7 Cu^{+2}	1009	1036	1124	1161
SIBS 62.8 Cu^{+2}	1007	1036	1126	1163
SIBS 94.9 Cu^{+2}	1007	1036	1126	1163
SIBS 29.7 K^{+1}	1009	1038	1126	1180
SIBS 62.8 K^{+1}	1009	1038	1126	1180
SIBS 94.9 K^{+1}	1009	1036	1126	1180

Permeability values were determined from the slope of $[(C_B(t)\ V_BL)/(C_AA)]$ versus time.

$$\frac{C_B(t)V_BL}{C_AA} = P\left(t - \frac{L^2}{6D}\right) \quad (2)$$

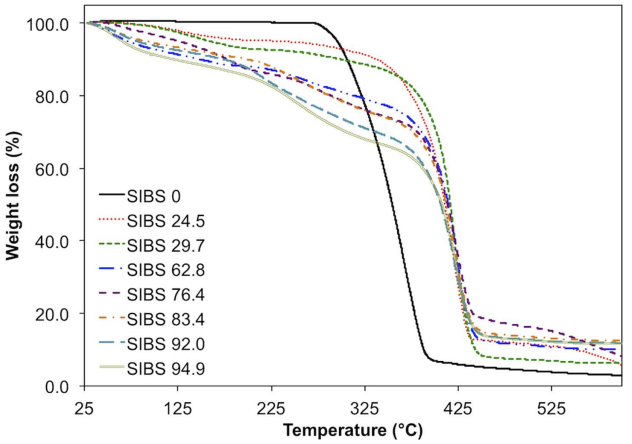

Figure 3. TGA curves for SIBS at various sulfonation levels. [Color figure can be viewed in the online issue, which is available at wileyonlinelibrary.com.]

Table IV. Degradation Temperatures for SIBS at Various Sulfonation Levels

Sample	Degradation temperatures (°C)	
	Sulfonic group	Backbone
SIBS 0	-	365.39
SIBS 24.5	-	418.08
SIBS 29.7	-	422.96
SIBS 62.8	276.31	422.71
SIBS 76.4	277.45	425.40
SIBS 83.4	251.64	421.08
SIBS 88.5	249.21	426.86
SIBS 90.4	235.49	422.67
SIBS 91.1	232.05	424.27
SIBS 92.0	221.63	420.50
SIBS 94.9	247.68	422.71

Table V. Degradation Temperatures for SIBS Cross-linked Membranes

Sample	Degradation temperatures (°C)		
	Sulfonic group	Backbone	Cations
SIBS 24.5	-	418.08	-
SIBS 24.5 Ba^{+2}	331	411.06	543.29
SIBS 24.5 Ca^{+2}	-	431.95	568.28
SIBS 24.5 Mg^{+2}	-	411.04	556.77
SIBS 24.5 K^{+1}	-	416.91	520.37
SIBS 24.5 Mn^{+2}	-	422.14	532.43
SIBS 24.5 Cu^{+2}	301.75	424.55	-
SIBS 62.8	276.31	422.71	-
SIBS 62.8 Ba^{+2}	-	412.21	467.01/537.71
SIBS 62.8 Ca^{+2}	-	420.28	495.20/552.07
SIBS 62.8 Mg^{+2}	-	413.96	473.40/569.8
SIBS 62.8 K^{+1}	-	414.99	437.20/512.48
SIBS 62.8 Mn^{+2}	-	413.31	474.80/554/49
SIBS 62.8 Cu^{+2}	307.74/385.13	424.87	-
SIBS 92.0	221.63	420.50	-
SIBS 92.0 Ba^{+2}	-	410.66	485.43/560.30
SIBS 92.0 Ca^{+2}	-	403.62	508.31/559.44
SIBS 92.0 Mg^{+2}	-	392.99	505.77/565.09
SIBS 92.0 K^{+1}	-	418.26	456.58/502.21
SIBS 92.0 Mn^{+2}	-	407.78	503.08/561.08
SIBS 92.0 Cu^{+2}	308.68/382.53	427.90	-

RESULTS AND DISCUSSION

Elemental Analysis

The sulfonation percent was calculated from the EA results of C H O S (Atlantic Microlab). The mole % sulfonation varied from 0 to 94.9% and as it will be explained ahead, FT-IR was used to confirm the location of the sulfonic groups in the polymer. INAA was used as an additional EA technique (Elemental Analysis) to confirm the consistency of the metal loading and to quantify the amount of cations in the polymer membranes. Table I shows the ratio of moles of metal per mole of sulfonic group in some of the polymer membranes studied. The results from Table I show two major effects: first, for each metal studied the mole ratio of metal to sulfonic group was very similar regardless of sulfonation level. Second, cations with a +2 charge have an average ratio of metal to sulfonic group that suggests one metal for every two sulfonic groups. For the only cation with +1 charge studied (K^{+1}), the ratio of metal to sulfonic group suggests one mole of metal for each mole of sulfonic group.

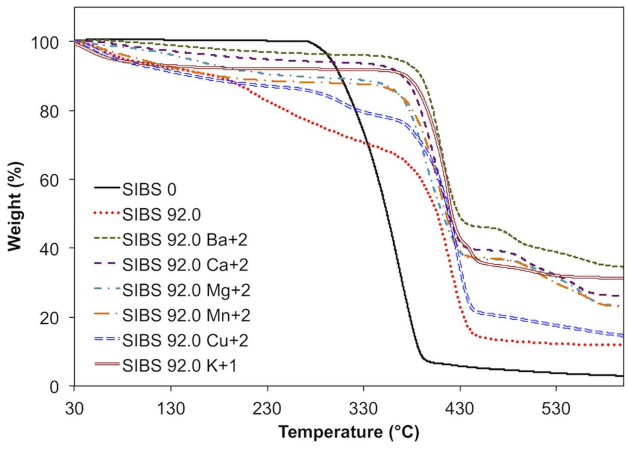

Figure 4. TGA curves for counter-ion substituted SIBS 92.0 membranes. [Color figure can be viewed in the online issue, which is available at wileyonlinelibrary.com.]

Ion Exchange Capacity

IEC was measured for the sulfonated membranes and the results are presented in Table II. The results suggest an optimum IEC with sulfonation level around 84.1% sulfonation. Beyond that sulfonation level the IEC is lower perhaps due to the formation of SO_2 bridges in the complex three-dimensional structure of the highly sulfonated polymer membranes.

Infrared Spectroscopy

Figure 1 shows the infrared spectrums of sulfonated SIBS, where SIBS 0 represents the unsulfonated polymer and SIBS 94.9 the highest sulfonation level studied. The spectra for the sulfonated polymers show four additional bands at high wavenumbers (marked with *: 1151, 1124, 1034, 1007 cm^{-1}), representative of the stretching vibrations associated to the sulfonate group. The bands at 1034 and 1151 cm^{-1} represent the symmetric and asymmetric SO_2 stretch, respectively. While at lower wavenumbers shows two bands at 698 and 756 cm^{-1} (marked with +), that correspond to the mono-substitution of the aromatic ring, that move and lower their intensity as the sulfonation level increase and one at 830 cm^{-1} (also marked +), that confirms the para- substitution of the sulfonate group on the aromatic ring. Figure 2 shows the spectrums of medium sulfonated counter-ion substituted membranes. The counter-ion substitution increases the intensity of the bands and shifts the asymmetric

Applied Polymer SCIENCE

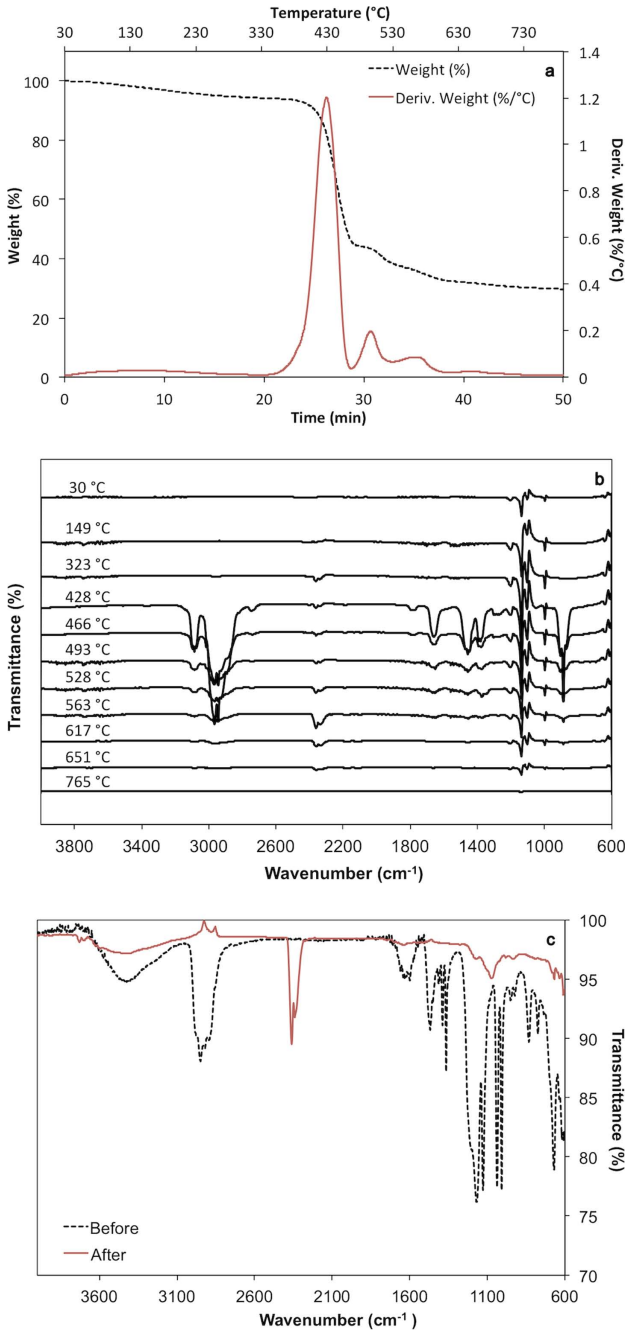

Figure 5. TGA-FTIR results for SIBS 92.0 cross-linked with Ba^{+2}: (a) Thermogravimetrical analysis results, (b) Infrared spectra as function of temperature, and (c) Infrared spectra before (dash line) and after (solid line) the thermogravimetrical analysis. [Color figure can be viewed in the online issue, which is available at wileyonlinelibrary.com.]

S—O stretching vibrations bands towards a higher wavenumber suggesting that the cations are interacting with the sulfonic groups in a way that more energy is required to obtain this stretching vibration. This effect is the same for all cations although the shifts are unique for each cation, especially for the asymmetric S—O stretching at 1151 cm^{-1} (Table III).

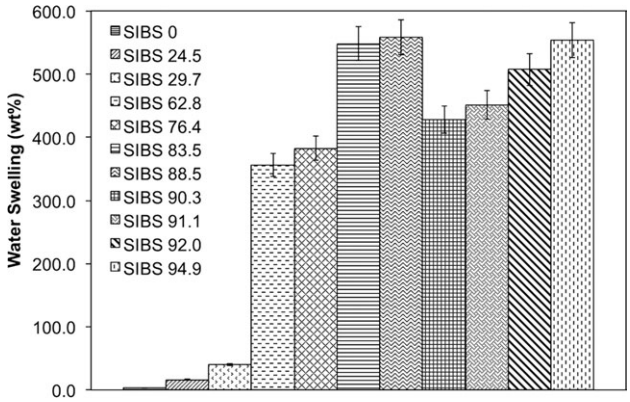

Figure 6. Water swelling experiments for SIBS at various sulfonation levels.

Thermogravimetrical Analysis

The thermogravimetric analysis (TGA) for unsulfonated and sulfonated SIBS is presented in Figure 3 and Table IV. On sulfonation the degradation temperature of the polymer backbone increases from 365 ± 1 to 422 ± 2°C regardless of sulfonation level. The TGA curves for the sulfonated SIBS show three weight loss stages, as it was demonstrated in previous studies.[2,30] The first region (50–200°C) is attributed to the atmospheric moisture absorbed by the hydroscopic ionic segments of the polymer and this region is left out of Table IV. The second (200–370°C) and third (370–430°C) are attributed to the breakdown of the sulfonic groups attached to the styrene ring and the degradation of the polymer backbone, respectively (Table IV). In many studies of block copolymers the degradation of the polymer has two components, one for each block (one for polystyrene and another polyisobutylene). In this case, only one band is observed for the degradation of the block copolymer. A previous study reports that these two bands may overlap and are indistinguishable from each other.[30]

The degradation temperature of the cation-substituted membranes is slightly different from the membranes in their acidic form (Figure 4 and Table V). The weight loss from 200 to 370°C is absent, but in all curves new degradation regions are

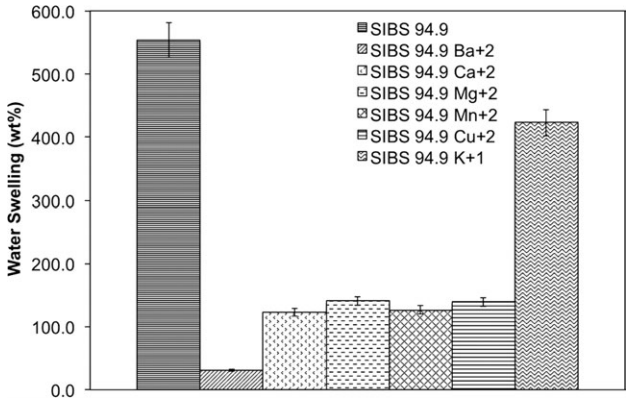

Figure 7. Water swelling experiments for counter-ion substituted SIBS 94.5 membranes.

Table VI. Water Absorption Limits (wt %) for SIBS Cross-linked Membranes

Sample	Sulfonated	Ba^{+2}	Ca^{+2}	Mg^{+2}	Mn^{+2}	$Cu+^{2}$	K^{+1}
SIBS 29.7	40.43	20.14	19.10	24.19	15.00	18.86	14.72
SIBS 62.8	355.83	26.43	73.41	75.60	82.87	77.67	284.66
SIBS 94.9	553.19	31.10	122.73	141.13	126.72	139.47	422.67

observed from 430 to 600°C. These new stages can be attributed to the decomposition of the sulfonic groups that are ionically associated to the counter-ions. The membranes cross-linked with Cu^{+2} show two new stages from 300 to 385°C that can also be associated to the sulfonic groups; however, the incorporation of this counter-ion makes the thermal stability of the ionic domains lower than the other counter-ions studied, perhaps because this atom has the highest electronegativity of all counter-ions studied. Detailed results for the degradation temperatures of the sulfonated and counter-ion substituted membranes are summarized in Tables IV and V.

TGA-FTIR

Figure 5(a) shows the TGA curve and its corresponding derivative curve for SIBS 92.0 substituted with Ba^{+2}, while Figure 5(b) shows the FTIR spectrums of the outlet gas of the TGA for this run as a function of temperature. From here we can confirm that the weight loss region around 370–430°C corresponds to the degradation of the polymer backbone chain. It is important to notice that for the Ba^{+2} substituted membranes 40% of the sample original weight remains thermally stable at 800°C; this is not the case for other membranes. FTIR spectrum for the sample after the TGA–FTIR experiment was obtained and compared with a previous spectrum obtained before the experiment [Figure 5(c)]. It is clear that some of the sulfonic group bands (1124, 1034 cm^{-1}) are missing and others have lowered their intensity suggesting that the cations may be interacting in different ways with the sulfonic groups.

Water Swelling

Figures 6 and 7 show the water absorption limits for sulfonated and counter-ion substituted SIBS membranes. All membranes reached their equilibrium water swelling in about 3 h; however, they were left longer (24 h) to guarantee equilibrium. Figure 6 also shows that the amount of water swelling increases with sulfonation level but up to a maximum, similar to the IEC results.

Table VII. Scattering Vector and Bragg Distance Values for the Sulfonated and Cross-linked Membranes

Sample	q^* (1/nm)	d_{Bragg} (nm)
SIBS 0	0.423	14.85
SIBS 29.7	0.362	17.36
SIBS 29.7 Ba^{+2}	0.362	17.36
SIBS 29.7 Ca^{+2}	0.362	17.36
SIBS 29.7 Mg^{+2}	0.362	17.36
SIBS 29.7 K^{+1}	0.362	17.36
SIBS 62.8	0.342	18.37
SIBS 94.9	0.285	22.05

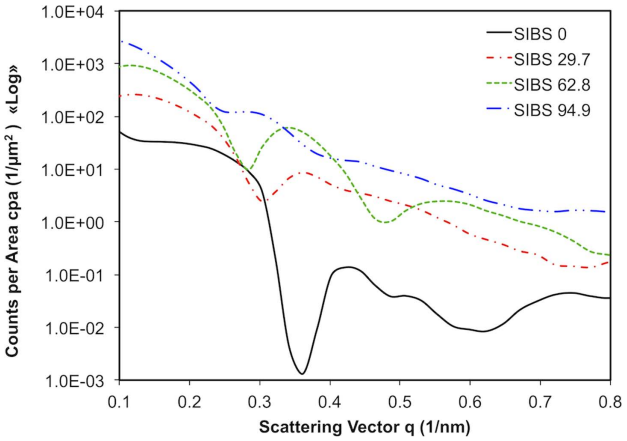

Figure 8. SAXS profiles for SIBS at various sulfonation levels. [Color figure can be viewed in the online issue, which is available at wileyonlinelibrary.com.]

The largest amount of water swelling (up to 558.5 wt %) was obtained with SIBS 88.5, the highest IEC (not sulfonation level). Above that sulfonation level, water swelling decreases perhaps because above that level there are additional interconnected bridges in the three-dimensional structure that inhibit the accessibility to the ionic domains. The incorporation of counter-ions shows significant differences between the sulfonated and cross-linked membranes (Figure 7 and Table VI). As Figure 7 shows, cation substitution reduces the absorption of water and produces unique swelling for each one of the cations studied.

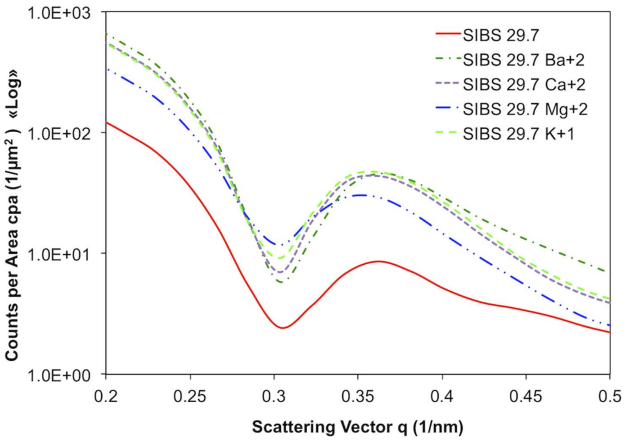

Figure 9. SAXS profiles for counter-ion substituted SIBS 29.7 membranes. [Color figure can be viewed in the online issue, which is available at wileyonlinelibrary.com.]

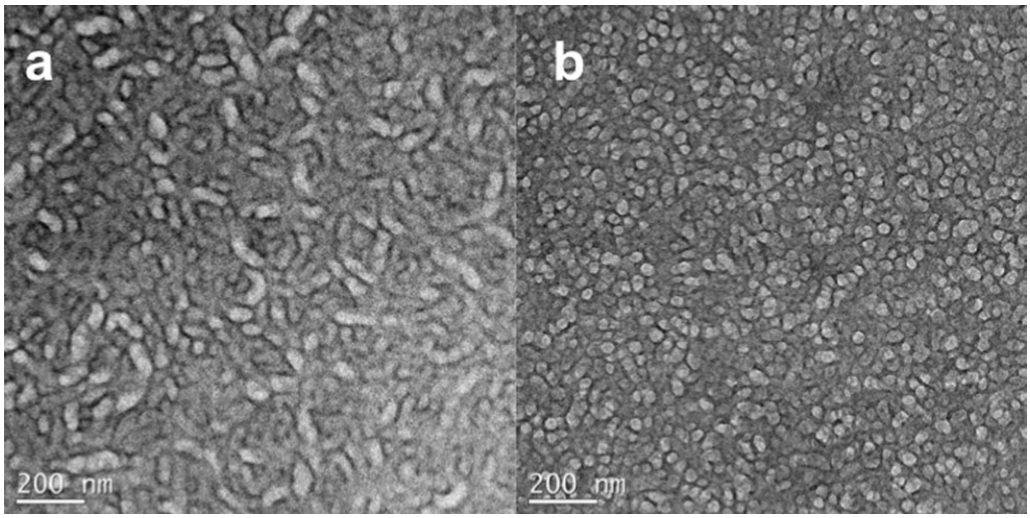

Figure 10. TEM images for: (a) SIBS 50.7 and (b) SIBS 89.7 membranes.

Small Angle X-Ray Scattering

Intensity profiles (I vs. q) were obtained normal to the plane for the sulfonated and counter-ion substituted membranes through SAXS experiments. The values of scattering vectors and interstitial (Bragg) distances for the ionic domains are shown in Table VII. The scattering vector, q, can be related to the interstitial distance between atoms using Bragg's Law[24,25]

$$d_{Bragg} = \frac{2\pi}{q_{Bragg}} \quad (3)$$

where d_{Bragg} is the distance between aligned atoms and q_{Bragg} is the scattering vector. Due to the weak scattering no periodic pattern was obtained, but the slopes of the curves suggested the presence of different morphologies (Figure 8). It is important to mention that as sulfonation increases, the Bragg distance between crystalline domains increases (Table VII). Counter-ion substituted SIBS 29.7 shows an increase in the intensity of the curve, but no significance difference in the interstitial distance for different cations, especially around the ionomer peak (Figure 9, Table VII). This suggests that the cations do not affect the size of the ionic nanochannels, but as it has been presented and will be presented ahead, they influence the equilibrium and transport properties through the membrane.

Transmission Electron Microscopy

TEM images of SIBS 50.7 and SIBS 89.7 are presented in Figure 10. The ionic nanochannels become more ordered and perpendicular to the surface as the sulfonation level increases (89.7%). The size of the ionic nanochannels observed agree with those obtained from Bragg's law and SAXS data. The lower sulfonation level shows more variations in the size and orientation of the ionic domains.

Transport Properties

Transport properties for protons (proton conductivity) and methanol (methanol permeability) were measured to evaluate the selectivity of the membranes with sulfonation level and counter-ion substitution. Proton conductivity was obtained from the real impedance component at high frequency of the Nyquist plot. A typical Nyquist plot with its corresponding regression is presented in Figure 11 for SIBS 84.1.

Proton conductivities for sulfonated and counter-ion substituted membranes are shown in Table VIII. The results show that proton conductivity increases with sulfonation level until it reaches a maximum (SIBS 84.1), like the IEC, suggesting a complex or non-oriented morphology at higher amounts of sulfonate groups. A possible explanation is that as the sulfonic groups increase, they interconnect among them forming well-defined ionic paths increasing the transport of protons across the membrane. At high sulfonation levels the interconnection among crystalline domains can occur in all directions and may create a random path that could cause the reduction in the transport of protons across the membrane. The incorporation of cations in the membranes reduced the proton conductivity regardless of sulfonation level (Table VIII). This decrease in the proton conductivity values for the cross-linked membranes was expected, since the cations are interacting with the sulfonic groups responsible for the transport of protons through the membrane.

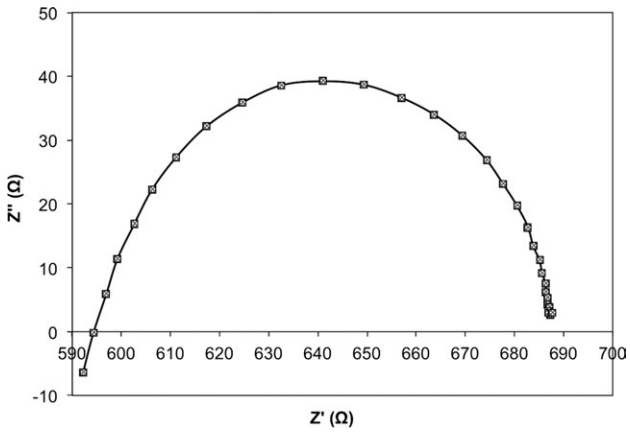

Figure 11. Nyquist plot with the circle fit regression where the low intercept represents the real impedance component for a SIBS 84.1 membrane.

Table VIII. Proton Conductivity Values (S/cm) for Sulfonated and Cross-linked SIBS Membranes

Sample	Sulfonated	Ba^{+2}	Ca^{+2}	Mg^{+2}	Mn^{+2}	Cu^{+2}	K^{+1}
SIBS 29.7	0.0317	0.0003	0.0011	0.0018	0.0012	0.0037	0.0076
SIBS 39.8	0.0479	0.0005	0.0042	0.0048	0.0048	0.0047	0.0169
SIBS 63.1	0.0906	0.0017	0.0099	0.0111	0.0115	0.0132	0.0322
SIBS 84.1	0.1050	0.0062	0.0270	0.0259	0.0265	0.0365	0.0459
SIBS 92.0	0.0888	0.0288	0.0321	0.0349	0.0247	0.0313	0.0526

However, another important variable for proton conductivity is the level of hydration. Figure 12 shows the proton conductivity of SIBS 84 dried and fully hydrated. The lack of water significantly reduces the proton conductivity and could be part of the reason for the reduction in the proton conductivity upon the incorporation of cations, since they also reduce the amount of water swelling in the membrane. Figure 12(b) shows that the proton conductivity is proportional to the water swelling of the membranes stressing the importance of water for the proton conductivity.

Methanol permeability follows the same behavior as proton conductivity and IEC; it increases until a specific sulfonation level (84.1%) is achieved and then decreases (Table IX). Methanol permeability also decreases upon the incorporation of counter-ions (Table IX). However, to evaluate differences between proton conductivity and methanol permeability with sulfonation level and counter-ion substitution these properties are presented differently (Figure 13). Figure 13(a) shows that proton conductivity seems to be proportional to IEC, while methanol permeability seems to increase exponentially with IEC. Beyond a critical IEC, the methanol permeability significantly increases. This difference might suggest an optimum IEC (e.g., 1.6) to maintain high proton conductivity and low methanol permeability. However it also emphasizes that there are fundamental differences in the transport mechanism of protons and methanol through sulfonated membranes.

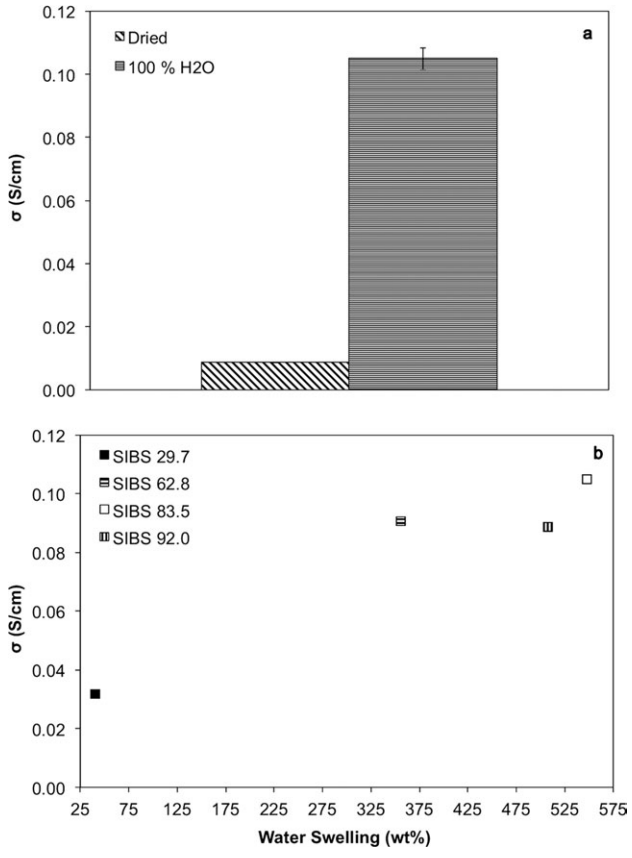

Figure 12. Proton conductivity (S/cm): (a) for dried and 100% hydrated sulfonated SIBS 84 membranes and (b) as a function of water swelling.

Figure 13(b) presents both properties versus counter-ion atomic radius. Methanol permeability seems to be more sensitive than proton conductivity to atomic size. Ba^{+2} and K^{+} are the two largest cations (217.4 and 227.2 pm, respectively); however, K^{+} does not reduce the proton conductivity or the methanol permeability as Ba^{+2}. K^{+} does not cross-link as Ba^{+2} does, indicated by the INNA results; this behavior results in K^{+} having a significantly higher amount of water swelling, which has been described as critical for proton conductivity and apparently is also important for methanol permeability. It should be pointed out that the size of the counter-ions (0.127–0.227 nm) is significantly lower than the size of the ionic nanochannels determined by SAXS (17–22 nm).

Selectivity

To analyze the effect of sulfonation and counter-ion substitution on the transport properties of protons and methanol, the

Table IX. Methanol Permeability (cm^2/s) and Normalized Selectivity Values for the Sulfonated and Cross-linked SIBS Membranes

Sample	Methanol permeability	STD deviation	Normalized selectivity
SIBS 29.7	1.49E-06	±7.78E-08	6.31E-01
SIBS 39.8	1.84E-06	±3.61E-07	7.71E-01
SIBS 63.1	5.75E-06	±1.98E-07	4.66E-01
SIBS 84.1	8.30E-06	±5.16e-07	3.74E-01
SIBS 84.1 Ba^{+2}	1.35E-06	±2.69E-07	1.36E-01
SIBS 84.1 Ca^{+2}	5.93E-06	±1.05E-06	1.35E-01
SIBS 84.1 Mg^{+2}	4.95E-06	±5.87E-07	1.55E-01
SIBS 84.1 K^{+1}	5.48E-06	±7.78e-07	2.48E-01
SIBS 84.1 Mn^{+2}	3.90E-06	±1.22E-06	2.01E-01
SIBS 84.1 Cu^{+2}	3.71E-06	±6.93E-07	2.91E-01
SIBS 92.0	3.42E-06	±2.97e-07	7.67E-01

Applied Polymer SCIENCE

membrane selectivity (α) (ratio of proton conductivity over methanol permeability) was calculated [eq. (4)]. The membrane selectivity represents the ability to allow transport of protons through the membrane, while blocking the passage of methanol.

$$\alpha = \frac{\sigma_{H_2}}{P_{MeOH}} \tag{4}$$

The selectivity reported for Nafion® 117 at ambient conditions is 3.38×10^4 S s/cm^3 ($P_{MeOH} = 1.98 \times 10^{-6}$ cm^2/s and $\sigma =$ 0.067 S/cm)[1]. To calibrate the changes in α with respect to the state-of-the-art Nafion®, a normalized selectivity (α^*) could be defined as the ratio of the measured selectivity divided by the Nafion® selectivity [eq. (5)].

$$\alpha^* = \frac{\left(\frac{\sigma_{H_2}}{P_{MeOH}}\right)_{SIBS}}{\left(\frac{\sigma_{H_2}}{P_{MeOH}}\right)_{Nafion\ 117}} \tag{5}$$

Figure 14 and Table IX show the normalized selectivity values obtained for sulfonated and counter-ion substituted SIBS. The selectivity of the SIBS membranes can be influenced by both sulfonation level and counter-ion substitution. Increasing the sulfonation level can increase IEC which influences water swelling, proton conductivity, and methanol permeability suggesting that the transport mechanism for protons and methanol through sulfonic nanochannels is similar. However, the magnitudes of the changes are different as methanol has a threshold above a certain IEC. Therefore, the best normalized selectivity (0.77) occurs for 39.8% and 92.0% sulfonation level (IEC = 1.06 and 1.57, respectively). The highest selectivities, although lower than Nafion®, are comparable (23% lower).

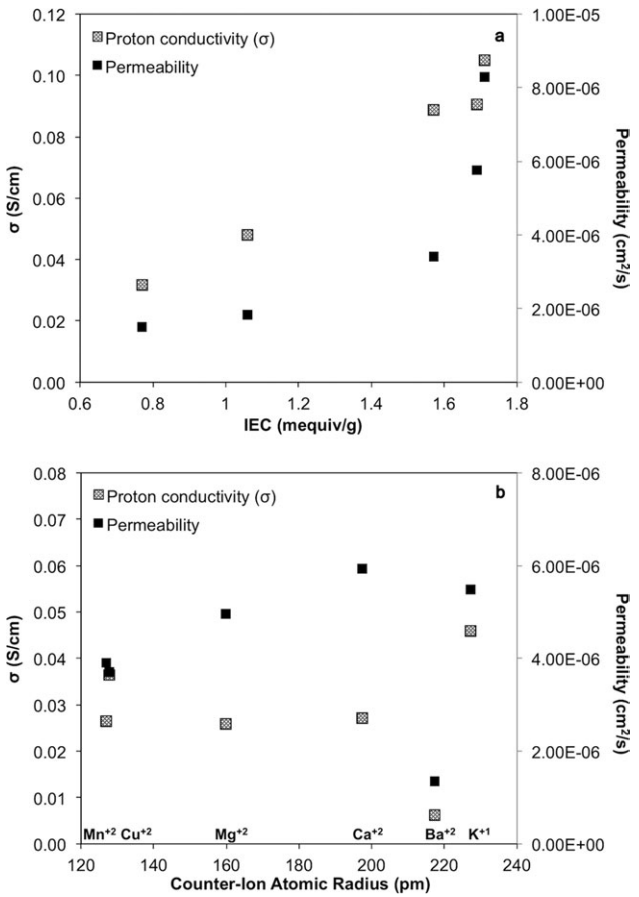

Figure 13. Proton conductivity and methanol permeability for: (a) SIBS as a function of IEC and (b) counter-on substituted SIBS 84.1 as a function of atomic radius.

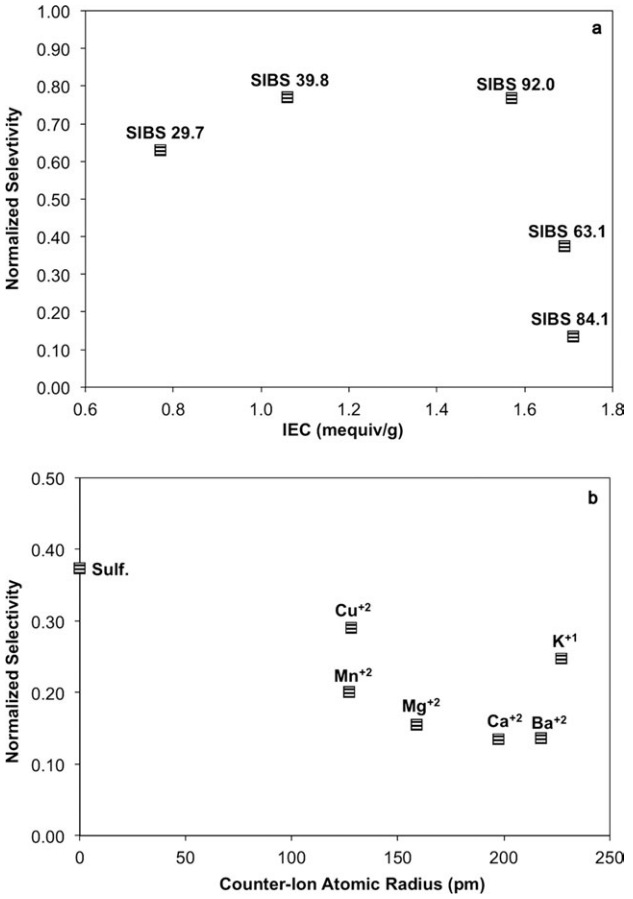

Figure 14. Normalized selectivity for: (a) SIBS as a function of IEC and (b) counter-ion substituted SIBS 84.1 as function of atomic radius.

The incorporation of counter-ion substitution into the sulfonated membranes, although maintain the size of the ionic nanochannels, reduces water swelling and also reduces both the proton conductivity and methanol permeability through the membrane therefore resulting in lower selectivity. However, the size of the counter-ion influences the methanol permeability more than the proton conductivity therefore resulting in unique selectivities [Figure 14(b) and Table IX]. K^+ behaves differently, since it is the only cation studied that does not cross-link and its hydration level is different than the other cations studied.

CONCLUSIONS

This investigation studied the equilibrium and transport properties of SIBS as a function of two major variables, sulfonation level and counter-ion substitution. Increasing sulfonation

increases IEC, which improves both the methanol permeability and the proton conductivity; however, the changes in proton conductivity and methanol permeability with IEC suggest fundamental differences in their transport mechanism worth studying further. Those differences lead to an optimum IEC for high proton conductivity and low methanol permeability.

The incorporation of counter-ions into the sulfonated membranes is limited by the nature of the metal and the interaction with the sulfonic group. The results suggest that for the +2 cations studied (Ba^{+2}, Ca^{+2}, Mg^{+2}, Mn^{+2}, Cu^{+2}) there is one mole of metal cross-linked for every two moles of sulfonic groups. The incorporation of the counter-ions into the sulfonic groups significantly reduces the methanol permeability responsible for the methanol cross-over limitation in direct methanol fuel cells, but it also reduces the proton conductivity. The reduction in the proton conductivity upon the incorporation of cations could be attributed to the reduction in the water absorbed, since the presence of water is critical for the transport of protons through PEM's. The reduction in methanol permeability upon the incorporation of counter-ions although is also sensitive to hydration level is more sensitive to the size of the counter-ion than the proton conductivity. These results support strong similarities in the transport mechanism of both protons and methanol through ionic nanochannels; however, they suggest that there might be additional fundamental differences in their transport mechanism worth studying further.

ACKNOWLEDGMENTS

This work was performed with the financial support of NSF under grants HRD-0833112 (CREST Program) and HRD-0832961 (PRLSAMP—BD Program), and DOD under grant W911-NF-11-1-0486. The authors acknowledge the support of Prof. Danilo C. Pozzo, of the University of Washington, where the SAXS experiments were conducted; Prof. Carlos Rinaldi, of the University of Puerto Rico at Mayaguez, for the FTIR facilities, Prof. Yossef Elabd, of Drexel University for the EIS facilities, and the Nanotechnology User Facility of the University of Washington (member of the National Nanotechnology Infrastructure Network) for the use of the TEM, especially to Scott Brasswell. Finally, the authors also acknowledge the help and support in the laboratory of Sully Mar Avilés, Emanuel Sánchez, Edward Guerrero, and David Mota.

REFERENCES

1. Elabd, Y. A.; Napadensky, E.; Sloan, J. M.; Crawford, D. M.; Walker, C. W. *J. Membr. Sci.* **2003**, *217*, 227.
2. Suleiman, D.; Elabd, Y. A.; Napadensky, E.; Sloan, J. M.; Crawford, D. M. *Thermochim. Acta* **2005**, *430*, 149.
3. Lu, X.; Wu, S.; Wang, L.; Su, Z. *Sensors Actuators B* **2005**, *107*, 812.
4. Sakthivel, M.; Weppner, W. *Sensors Actuators B* **2006**, *113*, 998.
5. Weng, Y.-C.; Hung, K.-C. *Sensors Actuators B*, **2009**, *141*, 161.
6. Peighambardoust, S. J.; Rowshanzamirand, S.; Amjadi, M. *Int. J. Hydrogen Energy* **2010**, *35*, 9349.
7. Wang, Y.; Chen, K. S.; Mishler, J.; Cho, S. C.; Adroher, X. C. *Appl. Energy* **2011**, *88*, 981.
8. Diaz, L. A.; Abuin, G. C.; Corti, H. R. *J. Membr. Sci.* **2012**, *411*, 35.
9. Duan, Q.; Wang, H.; Benziger, J. *J. Membr. Sci.*, **2012**, *392*, *393*, 88.
10. Tang, H.; Peikang, S.; Jiang, S. P.; Wang, F.; Pan M. *J. Power Sources* **2007**, *170*, 85.
11. Zhao, Y.; Yin, J. *Eur. Polym. J.* **2010**, *46*, 592.
12. Neburchilov, V.; Martin, J.; Wang, H.; Zhang, J. *J. Power Sources* **2007**, *169*, 221.
13. Adhikari, B.; Majumdar, S. *Prog. Polym. Sci.* **2004**, *29*, 699.
14. Wang, J. T.; Wainright, J. S.; Savinell, R. F.; Litt, M. *J. Appl. Electrochem.* **1996**, *26*, 751.
15. Fuller, J.; Breda, A. C.; Carlin, R. T. *J. Electrochem. Soc.*, **1997**, *144*, L67.
16. Gasa, J. V.; Weiss, R. A.; Shaw, M. T. *J. Membr. Sci.*, **2007**, *304*, 173.
17. Elamathi, S.; Nithyakalyani, G.; Sangeetha, D.; Ravichandran, S. *Ionics* **2008**, *14*, 377.
18. Park, C. H.; Lee, C. H.; Guiver, M. D.; Lee, Y. M. *Prog. Polym. Sci.* **2011**, *36*, 1443.
19. Bai, Z.; Durstock, M. F.; Dang, T. D. *J. Membr. Sci.* **2006**, *281*, 508.
20. Elabd, Y. A.; Napadensky, E. *Polymer* **2004**, *45*, 3037.
21. Silva, V. S.; Mendes, A.; Madeira, L. M.; Nunes, S. P. *J. Membr. Sci.*, **2006**, *276*, 126.
22. Elabd, Y. A.; Hickner, M. A.; *Macromolecules*, **2011**, *44*, 1.
23. Lawton, J. S.; Budil D. E. *Macromolecules*, **2009**, *43*, 652.
24. Storey, R. F.; Chisholm, B. J.; Masse M. A. *Polymer* **1996**, *37*, 2925.
25. Barreto, S. M. A.; Suleiman, D. *J. Membr. Sci.*, **2010**, *362*, 471.
26. Storey, R. F.; Baugh, D. W. *Polymer*, **2000**, *41*, 3205.
27. Chen, H.; Choi, J.-H.; Salas-de la Cruz, D.; Wineyand, K. I.; Elabd, Y. A. *Macromolecules*, **2009**, *42*, 4809.
28. Chen, L.; Hallinan, D. T.; Elabd, Y. A.; Hillmyer, M. A. *Macromolecules*, **2009**, *42*, 6075.
29. Crank, J. The Mathematics of Diffusion; Oxford University Press, **1975**; Chapter 44–51.
30. Suleiman, D.; Napadensky, E.; Sloan, J. M.; Crawford, D. M. *Thermochim. Acta* **2007**, *460*, 35.